Field dependence of the vortex core size probed by scanning tunneling microscopy

A. Fente, E. Herrera, I. Guillamón, and H. Suderow[*]

*Laboratorio de Bajas Temperaturas, Departamento de Física de la Materia Condensada, Instituto de Ciencia de Materiales Nicolás Cabrera
and Condensed Matter Physics Center (IFIMAC), Universidad Autónoma de Madrid, Spain
and Unidad Asociada de Bajas Temperaturas y Altos Campos Magnéticos, UAM, CSIC, Spain*

S. Mañas-Valero, M. Galbiati, and E. Coronado

Instituto de Ciencia Molecular (ICMol), Universidad de Valencia, Catedrático José Beltrán 2, 46980 Paterna, Spain

V. G. Kogan[†]

Ames Laboratory, US Department of Energy, Ames, Iowa 50011, USA

We study the spatial distribution of the density of states (DOS) at zero bias $N(\boldsymbol{r})$ in the mixed state of single and multigap superconductors. We provide an analytic expression for $N(\boldsymbol{r})$ based on deGennes' relationship between DOS and the order parameter that reproduces well scanning tunneling microscopy (STM) data in several superconducting materials. In the single gap superconductor β-Bi$_2$Pd, we find that $N(\boldsymbol{r})$ is governed by a length scale $\xi_H = \sqrt{\phi_0/2\pi H}$, which decreases in rising fields. The vortex core size $\mathcal{C}$, defined via the slope of the order parameter at the vortex center, $\mathcal{C} \propto (d\Delta/dr|_{r\to0})^{-1}$, differs from ξ_H by a material dependent numerical factor. The new data on the tunneling conductance and vortex lattice of the 2H-NbSe$_{1.8}$S$_{0.2}$ show the in-plane isotropic vortices, suggesting that substitutional scattering removes the in-plane anisotropy found in the two-gap superconductor 2H-NbSe$_2$. We fit the tunneling conductance of 2H-NbSe$_{1.8}$S$_{0.2}$ to a two gap model and calculate the vortex core size $\mathcal{C}$ for each band. We find that $\mathcal{C}$ is field independent and has the same value for both bands. We also analyze the two-band superconductor 2H-NbS$_2$ and find the same result. We conclude that, independently of the magnetic field induced variation of the order parameter values in both bands, the spatial variation of the order parameter close to the vortex core is the same for all bands.

I. INTRODUCTION

The spatial distribution of the quasiparticles density of states (DOS) within the vortex lattice (VL) is intimately related to the spatial distribution of the order parameter. The latter is governed by the coherence length ξ which sets the size of the vortex core and by the applied magnetic field which fixes the intervortex spacing.

There are a few definitions of ξ used in literature, adjusted to a particular problem at hand, see, e.g., Ref. [1]. Within this work, ξ is associated with the vortex core size $\mathcal{C}$, which is related to the order parameter slope at the vortex center, $d\Delta/dr|_{r\to0} \propto 1/\xi \propto 1/\mathcal{C}$. It was suggested theoretically that $\mathcal{C}$ shrinks with the increasing magnetic field H [1]. Basically, the coherence length ξ (along with the core size) is not among the input parameters of the BCS theory—it should be evaluated and this is a nontrivial task. The evaluation done on quite general grounds in Ref. [1] (and in works cited therein) has shown that in clean isotropic materials the H dependence of $\mathcal{C}$ is close to $1/\sqrt{H}$ in large fields.

In fact, interpreting μSR data on various materials, it was deduced that ξ decreases with increasing fields following roughly the $1/\sqrt{H}$ dependence [2]. This conclusion was obtained with the help of London-based models for the field distribution within VL. In these models, ξ enters as a cutoff restricting their applicability. For this reason, extracting $\xi(H)$

from μSR data can hardly be considered as direct. Similar shortcomings can be attributed to $\xi(H)$ deduced from the magnetization data [3].

The scanning tunneling microscopy (STM) has the advantage of directly probing the spatial distribution of the quasiparticles DOS within the vortex lattice. The DOS depends on the value of the order parameter $\Delta(\boldsymbol{r})$ and can be used, in principle, to map $|\Delta(\boldsymbol{r})|$ within VL. This was done within the microscopic quasiclassical formalism by U. Klein [4] for clean Nb, by N. Nakai *et al* for 2H-NbSe$_2$ [5], and by F. Gygi and M. Schlüter using Bogolyubov-deGennes formalism [6]. Similar approaches have been applied to nickel-borocarbides and pnictide compounds [7–9], requiring detailed knowledge of the normal phase properties [8–11]. However, extracting a value for ξ or obtaining order parameter variations in different bands from STM data remains highly nontrivial. There is thus a need to discuss within a simple model the spatial distribution of the DOS within vortex lattices.

Perhaps the most compact and simple result for the DOS distribution in the mixed state was given by P.G. deGennes in the work on dirty superconductors [12,13]. Following this work, we offer here a phenomenological scheme to describe the STM data on zero-energy DOS for materials with hexagonal vortex lattices. If needed, the approach can be generalized for other VL symmetries and for anisotropic superconductors. We show that the DOS distribution within VL can be well described by the model for single- and two-gap superconductors. For the single-gap case we find that the core size $\mathcal{C}$ is proportional to a universal length $\xi_H = \sqrt{\phi_0/2\pi H}$. When H approaches the upper critical field H_{c2}, ξ_H coincides

[*]Corresponding author: hermann.suderow@uam.es
[†]Corresponding author: kogan@ameslab.gov

TABLE I. Superconducting parameters of the compounds studied. The gap values are obtained from the fits (red lines in Fig. 1), see Table II in Appendix A.

Compound	T_c (K)	H_{c2} (T)	ξ_{c2} (nm)	Δ (meV)
β-Bi$_2$Pd	5	0.6	23	0.8
2H-NbSe$_{1.8}$S$_{0.2}$	7	7	7	0.8; 1
2H-NbS$_2$	5.7	2.5	12	0.5; 1

with the commonly used coherence length $\xi_{c2} = \sqrt{\phi_0/2\pi H_{c2}}$. This behavior agrees with predictions [1] for clean materials. For the two-gap samples, we find nearly field independent and equal core sizes, $\mathcal{C}_1 = \mathcal{C}_2$.

II. EXPERIMENTAL

We have chosen β-Bi$_2$Pd for a single gap superconductor, and 2H-NbSe$_{1.8}$S$_{0.2}$ and 2H-NbS$_2$ which are multigap superconductors with no in-plane anisotropy. The tunneling conductance and VL in 2H-NbSe$_{1.8}$S$_{0.2}$ is first reported here, whereas the data for β-Bi$_2$Pd and 2H-NbS$_2$ are taken from our previous work [14,15]. Details of the sample preparation and of DOS measurements are given in Appendices A and C. Superconducting parameters of the compounds are given in Table I, and their zero-field tunneling conductance curves are shown in Fig. 1. Note that the critical temperatures of the three compounds are similar, although ξ_{c2} obtained from the upper critical fields vary by a factor of three. Mean free paths have been estimated from resistivity measurements, yielding values slightly above or comparable to the coherence lengths. β-Bi$_2$Pd is clearly a single gap superconductor ($\Delta = 0.76$ meV, Fig. 1) with a zero field conductance following s-wave BCS theory and shows a hexagonal VL [14]. The zero-field conductance of both 2H-NbSe$_{1.8}$S$_{0.2}$ and 2H-NbS$_2$ can be fitted using BCS theory (red lines in Fig. 1) with two gaps (see Table I) [10,11,16].

To obtain tunneling conductance vs distance from the vortex center, we select single vortices out of zero-bias conductance images and evaluate angular averages of the normalized conductance σ_0 for each r. We define σ as:

$$\sigma = \frac{\sigma_0(r) - \sigma_0(r^*)}{\sigma_0(0) - \sigma_0(r^*)}, \qquad (1)$$

where r^* is the distance from the vortex center to the point where the tunneling conductance is minimum (in the hexagonal lattice, the center of an equilateral vortex triangle).

III. MODEL

The zero-bias DOS, $N(\boldsymbol{r})$, in large fields of the mixed state at low temperatures and in the dirty limit was given by P.G. deGennes [12,17]:

$$\frac{N(\boldsymbol{r})}{N_n} = 1 - \frac{|\Delta(\boldsymbol{r})|^2}{\Delta_0^2}. \qquad (2)$$

N_n is DOS in the normal phase. Note that this relation does not account for possible core states [18], in other words, we disregard the effect of these states on the shape of $|\Delta(\boldsymbol{r})|$, which acts as an effective potential due to which the bound
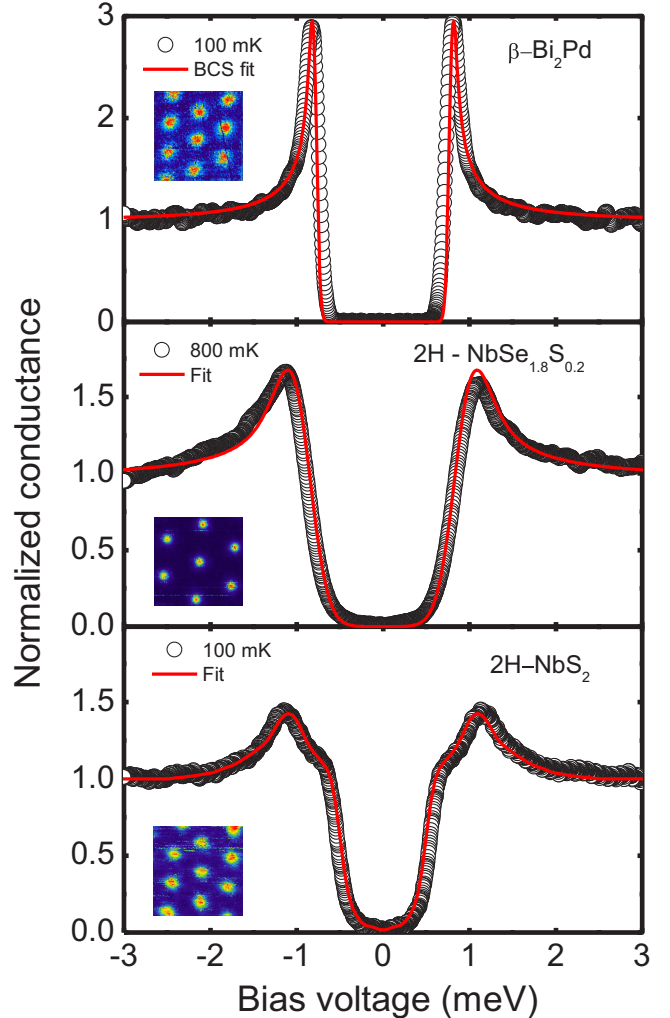

FIG. 1. Zero field tunneling conductance for β-Bi$_2$Pd (upper panel), 2H-NbSe$_{1.8}$S$_{0.2}$ (middle panel), and 2H-NbS$_2$ (lower panel). Fits to BCS theory are given by red lines (see also Table II in Appendix A). Temperatures at which the data were taken are given in each panel. Insets show VL images obtained from the zero-bias conductance at, from top to bottom, 0.05 T, 0.1 T, and 0.15 T (lateral sizes of the images are 450 nm, 360 nm, and 290 nm, respectively).

core states are formed. When $\Delta \rightarrow 0$, as, e.g., at H_{c2} or at vortex centers, $N \rightarrow N_n$ as it should. This remarkable relation expresses the local DOS in terms of the order parameter at the same point. Precise value of the constant Δ_0 (on the order of zero-T BCS gap) will not affect our analysis.

TABLE II. Superconducting parameters of the compounds studied used to obtain the red lines in Fig. 1; Γ's are the broadening parameters.

Compound	$\Delta_{1,2}$ (meV)	$\Gamma_{1,2}$ (meV)
β-Bi$_2$Pd	0.76, -	-,-
2H-NbSe$_{1.8}$S$_{0.2}$	0.78, 1	0.12, 0.12
2H-NbS$_2$	0.5, 1	0.16, 0.22

One can argue that $N(r)$ depends only on even powers of Δ. Within the Eilenberger version of the BCS theory [19] the superconductivity is described by Gor'kov Green's functions integrated over energy, f, f^+, and g, which depend on Matsubara frequencies ω and are related by $g^2 = 1 - ff^+$. The DOS as a function of energy ϵ is given by $N = N_n \mathrm{Re}[g(\omega \to i\epsilon)]$, where f and f^+ are $\propto |\Delta|$. Hence, g depends only on $|\Delta|^2$ and so does N.

In large fields of the mixed state even between vortices, the order parameter is suppressed relative to the zero-field value Δ_0. The ratio $\Delta^2(r)/\Delta_0^2$ is small and terms correcting Eq. (2) of the order $\Delta^4(r)/\Delta_0^4$ are smaller yet. Hence, Eq. (2) is likely to hold not only in the dirty limit [20], and we take it as a basis of our phenomenological model.

The order parameter for a single vortex in isotropic superconductors can be approximated by [21,22]:

$$\frac{\Delta(r)}{\Delta_0(T)} = \frac{r}{\sqrt{r^2 + \mathcal{C}^2}}, \qquad (3)$$

where the core size $\mathcal{C}$ is of the order of ξ. This function reproduces the expected behavior for $r \to 0$, where $d\Delta/dr|_{r\to 0} = \Delta_0/\mathcal{C}$; for $r \gg \mathcal{C}$, $\Delta \to \Delta_0$, the order parameter of uniform zero-field state. Minimizing the Ginzburg-Landau energy functional, Z. Hao and J. Clem deduced $\mathcal{C} = \xi\sqrt{2}$ to fit magnetization data in large fields [23].

For the hexagonal VL of our samples, the unit cell can be taken as a hexagon centered at the vortex. Hence, we can use Wigner-Seitz approximation and consider the unit cell as a circle of a radius a such that $\pi a^2 = \phi_0/B$, ϕ_0 is the flux quantum, and B is the magnetic induction. For platelike samples we work with, in fields perpendicular to plates faces, B is close to the applied field H. The cell radius a is close to half of the intervortex distance L: $2a/L = (2\sqrt{3}/\pi)^{1/2} \approx 1.05$.

To satisfy the periodicity condition, the normal derivative of $|\Delta|$ should vanish at the unit cell boundary. Within circular approximation this translates to $d\Delta/dr = 0$ at the boundary $r = a$. The function (3) does not satisfy this condition, although for $a \gg \mathcal{C}$ this derivative is small. To correct this, we modify the form (3) to

$$\frac{\Delta(r)}{\Delta_0(B,T)} = \frac{r}{\sqrt{r^2 + \mathcal{C}^2}} \exp\left[-\frac{r^2 \mathcal{C}^2}{2a^2(\mathcal{C}^2 + a^2)}\right], \qquad (4)$$

which satisfies $d\Delta/dr = 0$ at $r = a$; for $a \gg \mathcal{C}$ it approaches the maximum at the cell boundary exponentially slowly. Expressions (3) and (4) practically coincide within the core $r < \mathcal{C}$; for larger r the new function varies slower than for a single vortex. The slope $d\Delta/dr|_{r\to 0} = \Delta_0/\mathcal{C}$, so that $\mathcal{C}$ can still be taken as the core size.

Next, we observe that the normalizing constant $\Delta_0(B,T)$ drops off the measured quantity

$$\sigma = \frac{N(r) - N(a)}{N(0) - N(a)} = \frac{\Delta^2(a) - \Delta^2(r)}{\Delta^2(a) - \Delta^2(0)} = 1 - \frac{\Delta^2(r)}{\Delta^2(a)} \qquad (5)$$

since $\Delta(0) = 0$. We now take a as a unit length to obtain:

$$\sigma = 1 - \frac{\rho^2(1 + \eta^2)}{\rho^2 + \eta^2} \exp\frac{\eta^2(1 - \rho^2)}{1 + \eta^2},$$
$$\rho = r/a, \qquad \eta = \mathcal{C}/a. \qquad (6)$$

IV. RESULTS

A. β-Bi$_2$Pd

Let us first focus on β-Bi$_2$Pd (Fig. 2). Fitting the data to Eq. (6) and treating η as a fit parameter we can extract the core size $\mathcal{C}$. The good quality of the fit validates our model as able to provide quantitative description of the STM data. The fits yield values of η around 0.50 ± 0.08 in a field range where H
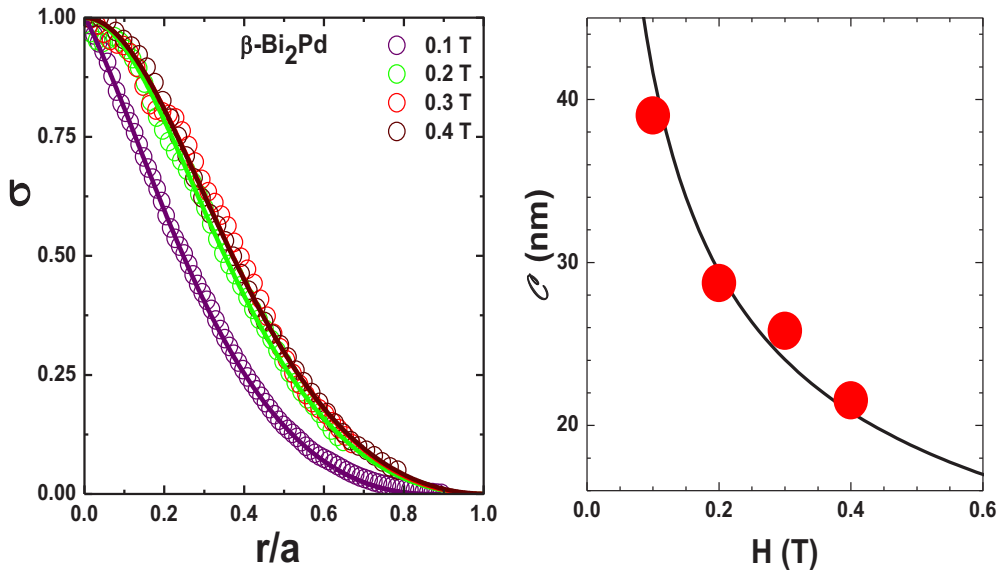

FIG. 2. The left panel: the tunneling conductance σ of Eq. (5) vs distance r from the vortex center, normalized to the cell radius a, for β-Bi$_2$Pd and in fields indicated. Data are taken at 0.15 K and have been obtained from images of vortices averaged over the angle for each r and normalized as described in the text. The right panel: the core size $\mathcal{C}$ of Eq. (7) vs H. Dots are the values of $\mathcal{C} = \eta a$ obtained from the fits of the left panel with a being the Wigner-Seitz cell size. The line is $\mathcal{C}$ calculated with $\eta \approx 0.5$ found in the fits.
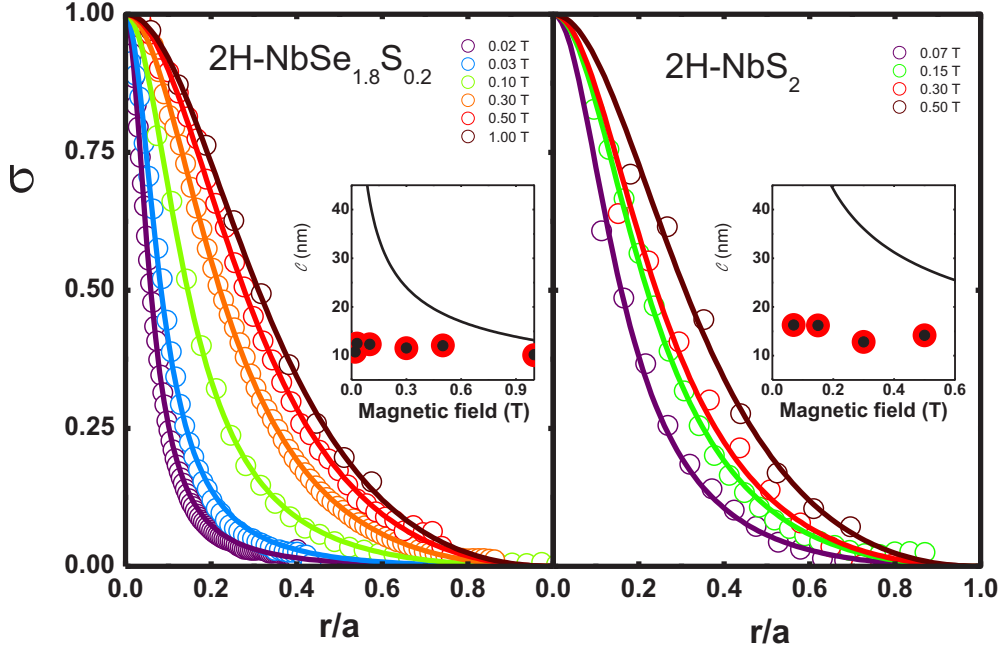
FIG. 3. Normalized conductance σ for 2H-NbSe$_{1.8}$S$_{0.2}$ (left panel) and for 2H-NbS$_2$ (right panel). Lines are fits as described in the text. Insets give the core size vs magnetic field $\mathcal{C}_{1,2}$ (red and black points, respectively) and the line is $\mathcal{C}$ calculated with $\eta \approx 0.5$ for comparison.

changes by a factor of 4. Since $\eta \approx$ const, we have

$$\mathcal{C} = \eta a = \eta \sqrt{\frac{\phi_0}{\pi H}}. \qquad (7)$$

Hence, the core size $\mathcal{C}$ varies with applied field as $1/\sqrt{H}$, the dependence deduced from the μSR data on many materials [2]. This is highlighted by the red points in the right panel of Fig. 2, which provide $\mathcal{C}$ vs magnetic field.

The theory of Ref. [1] suggests that in large fields the coherence length as a function of field should behave as $\xi \approx A/\sqrt{H}$ (except in the extreme dirty limit or at high temperatures). In particular, this relation should hold at the upper critical field H_{c2}. This gives the constant $A = \sqrt{\phi_0/2\pi}$ so that we have

$$\xi = \sqrt{\frac{\phi_0}{2\pi H}} \equiv \xi_H. \qquad (8)$$

The core size, therefore, is

$$\mathcal{C} = \eta a = \eta \sqrt{\frac{\phi_0}{\pi H}} = \eta \sqrt{2} \xi_H. \qquad (9)$$

Using $\eta \approx 0.5$ obtained by the fits, we find $\mathcal{C} \approx 0.7 \xi_H$. Equation (9) implies that the order parameter and DOS distributions within VL in large fields of one-band isotropic materials are governed by a *universal* length ξ_H of Eq. (8). As $H \to H_{c2}$, ξ_H reaches the value of the standard coherence length $\xi_{c2} = \sqrt{\phi_0/2\pi H_{c2}}$. Our results suggest that by a proper rescaling, distributions of zero-bias DOS in large-field vortex lattices in one-band isotropic superconductors can be reduced to a nearly universal form.

B. 2H-NbS$_2$ and 2H-NbSe$_{1.99}$S$_{0.01}$

We now turn to multigap superconductors 2H-NbSe$_{1.8}$S$_{0.2}$ and 2H-NbS$_2$. To generalize our model to the two-gap situation

we assume that the order parameter takes values Δ_1 and Δ_2 on two bands and write the spatially dependent density of states as

$$\frac{N(\boldsymbol{r})}{N_n} = 1 - n_1 \frac{\Delta_1^2(\boldsymbol{r})}{\Delta_{10}^2} - n_2 \frac{\Delta_2^2(\boldsymbol{r})}{\Delta_{20}^2}, \qquad (10)$$

where $n_{1,2}$ are partial DOS in the normal state, $n_1 + n_2 = 1$. Each Δ_ν ($\nu = 1,2$) satisfies the boundary condition $d\Delta_\nu/dr = 0$ at the cell boundary $r = a$, because each one should be periodic in the vortex lattice:

$$\frac{\Delta_\nu(\boldsymbol{r})}{\Delta_{0\nu}} = \delta_\nu = \frac{\rho}{\sqrt{\rho^2 + \eta_\nu^2}} \exp\left[-\frac{\rho^2 \eta_\nu^2}{2(\eta_\nu^2 + 1)} \right], \qquad (11)$$

$\eta_\nu = \mathcal{C}_\nu/a$, $\nu = 1,2$. Note that δ_ν are normalized to corresponding $\Delta_{0\nu}$. Substituting this in Eq. (10), we obtain:

$$\sigma = 1 - \frac{\delta_1^2(\rho) + \gamma \delta_2^2(\rho)}{\delta_1^2(1) + \gamma \delta_2^2(1)}, \quad \gamma = \frac{n_2}{n_1}. \qquad (12)$$

Fitting the data for $\sigma(r)$ we extract η_1 and η_2. Figure 3 shows results of such a fitting. The good quality of the fits is remarkable. Thus, the expression (12) describes well the spatial distribution of the DOS in two-gap systems. Using Eq. (10), we calculate the core sizes from the fitting parameters and find—within the accuracy of our procedure—nearly equal and field independent core sizes $\mathcal{C}_1$ and $\mathcal{C}_2$.

The spatial dependence of the conductance curves in 2H-NbSe$_{1.8}$S$_{0.2}$ and in 2H-NbS$_2$, plotted vs r/a, is clearly H dependent (Fig. 3). The density of states spreads considerably when applying magnetic field, i.e., the parameters η_ν increase with the magnetic field. This means that $\mathcal{C} = \eta a$ no longer shrinks with the increasing vortex density, in fact the fits show that $\mathcal{C}$ is field independent. What is more, the slopes of the order parameter values in the vortex center, $\mathcal{C}_1$ and $\mathcal{C}_2$, in each of the two bands remain the same.

Let us now discuss the magnetic field independence of $\mathcal{C}$. This is expected for one-band superconductors in the dirty limit [1]. In 2H-NbSe$_{1.8}$S$_{0.2}$, there is a remarkable increase of H_{c2} by a factor of two with respect to pure 2H-NbSe$_2$, and the zero bias peak at the vortex core is considerably suppressed (see Appendix B). The Fermi velocities range from 10^5 m/s to well above 10^6 m/s, leading to BCS zero-T coherence length values between 10 nm and 50 nm, in any case above the values $\xi_{c2} \approx 7$ nm obtained from H_{c2} (see Table I) [24,25]. This suggests that the influence of scattering is strong in 2H-NbSe$_{1.8}$S$_{0.2}$.

In 2H-NbS$_2$, the residual resistivity is the lowest among the compounds discussed here (see Appendix D), and there is a clear zero-bias peak at the vortex core, comparable to the peak observed in pure 2H-NbSe$_2$ [15]. The observed magnetic field independence of $\mathcal{C}$ is therefore unexpected in this material and requires more careful band dependent calculations. Probably, the scattering is band dependent, giving different sensitivities to scattering on the zero-bias peak and the spatial dependence of the order parameter in vortex cores.

On the other hand, our model applied to STM data on two-gap 2H-NbSe$_{1.8}$S$_{0.2}$ and 2H-NbS$_2$ shows that the length scales on which the order parameter changes in the two bands are, in fact, the same. This outcome is unexpected, one would think that at low temperatures the length scales at which order parameters change should be close to the BCS coherence lengths of the two bands, $\xi_{0v} \propto v_v/T_c$. However, it has been shown time ago by B. Geilikman, R. Zaitsev, and V. Kresin [26] and "rediscovered" recently [27,28] that near T_c the two-gap Ginzburg-Landau theory yields the same length scales for variation of both Δ_1 and Δ_2. Our conclusion that the same is true for low temperatures in materials examined is, of course, based on phenomenological model. The model, however, should not be far from reality since we are able to reproduce low temperature STM data quite well. On the theoretical side, calculations based on Bogolyubov-deGennes formalism showed different low temperature ξ's in two bands for a weak interband coupling [29]. This suggests that in materials examined here, the interband coupling is not weak. Altogether, the question of the microscopic conditions for having $\xi_1 = \xi_2$ at low temperatures is still open.

To summarize, we argue that the deGennes formula for the zero-bias DOS $N(\boldsymbol{r})$ in the mixed state [12] can be used out of the dirty limit. Combining this with the Wigner-Seitz approximation for the order parameter within the VL unit cell and the known approximation for the order parameter distribution, we are able to reproduce the experimental $N(\boldsymbol{r})$ for one- and two-gap materials. This allows us to extract the vortex core size $\mathcal{C}$ not as an imaginary boundary separating the "normal" core from superconducting environment, but as a parameter characterizing the DOS distribution in the vortex lattice. We find that the core size in the isotropic material β-Bi$_2$Pd shrinks as $1/\sqrt{H}$ as predicted in Ref. [1] for the clean limit, whereas it remains H independent in multigap cases of 2H-NbSe$_{1.8}$S$_{0.2}$ and 2H-NbS$_2$. In 2H-NbSe$_{1.8}$S$_{0.2}$, scattering leads to the H independent core size expected in Ref. [1] for the dirty limit. The result in 2H-NbS$_2$ suggests that the band dependence of electronic scattering is important

to understand details of the density of states of multigap superconductors. Furthermore, in the latter two compounds, we find no difference between the magnetic field dependence of the core size in both bands.

APPENDIX A: VORTEX LATTICE OF 2H-NbSe$_{1.8}$S$_{0.2}$

The experiment consists of a home built low-noise dilution refrigerator STM system as described in Refs. [30,31]. The tunneling conductance curves are taken with an energy resolution of about 15 μeV [32,33]. We use an Au tip, which is cleaned by repeated indentation onto the Au cleaning pad [34]. The samples were cleaved *in situ* to obtain fresh surfaces. Atomic resolution was consistently achieved in all compounds discussed in this paper. The magnetic field is applied perpendicular to the platelike samples. At the measurement temperature (of 0.15 K for β-Bi$_2$Pd, 0.1 K for 2H-NbS$_2$, and 0.8 K for 2H-NbSe$_{1.8}$S$_{0.2}$) we can safely assume that the local conductance is proportional to the local DOS, so that we can replace the measured conductance σ_0 with the DOS N's. To make the fits shown in the main text (red lines of Fig. 1), we use a single gap fit for β-Bi$_2$Pd and two gaps $\Delta_{1,2}$ for the rest of the samples with a Gaussian smearing of the DOS having a width of $\Gamma_{1,2}$ (see Table I).

A few images of isolated vortices and of the vortex lattice in 2H-NbSe$_{1.8}$S$_{0.2}$ are shown in the left panels of Fig. 4 for a set of magnetic fields. The right panels show the evolution of the images with changing bias voltage at $H = 0.3$ T. Note that, contrary to the much discussed case of star-shaped vortices in
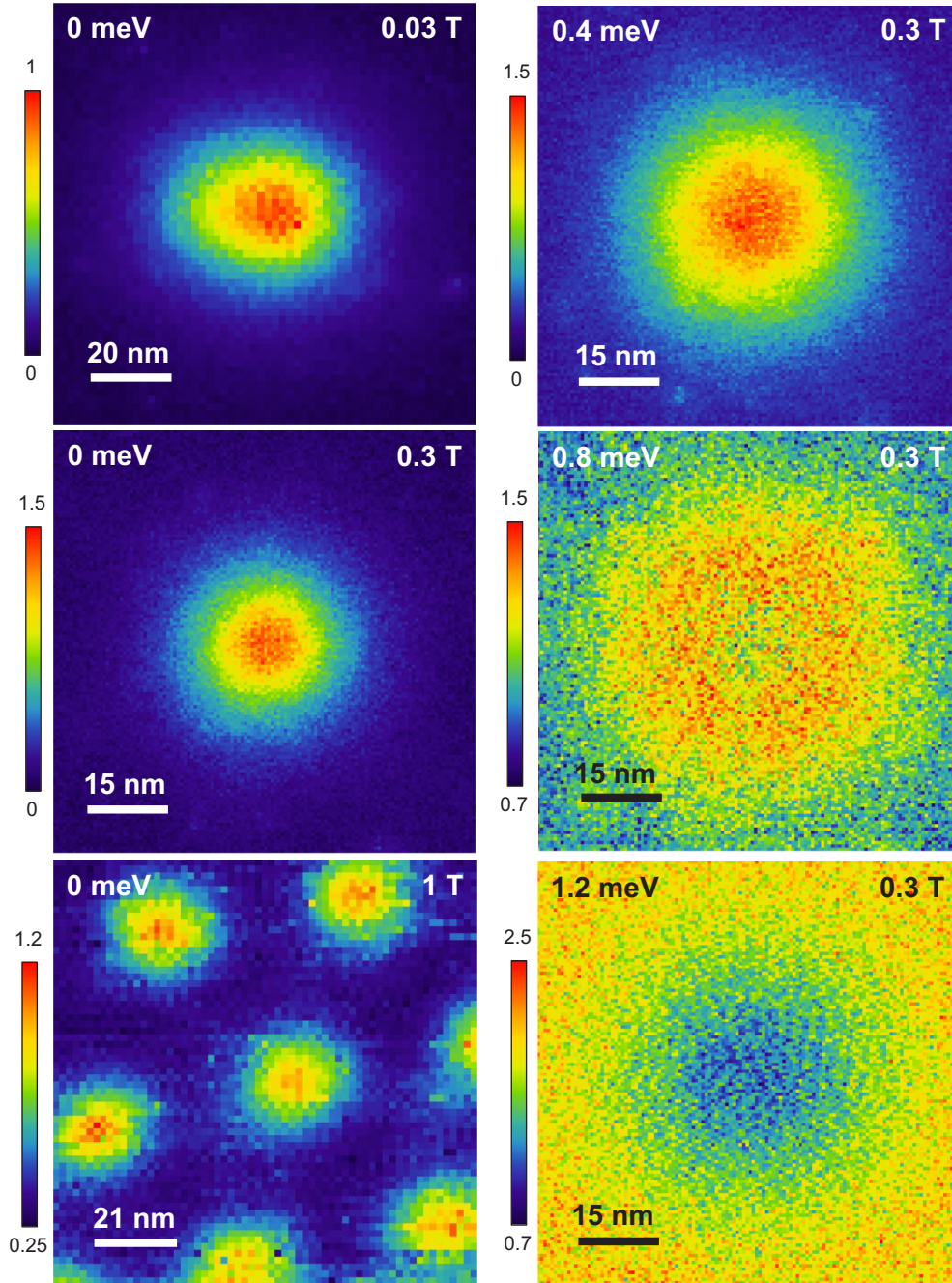
FIG. 4. Left panels: the zero-bias conductance maps in 2H-NbSe$_{1.8}$S$_{0.2}$ at $T = 0.8$ K at fields indicated. Right panels: conductance maps of an isolated vortex for bias voltages indicated and a magnetic field of 0.3 T.

2H-NbSe$_2$, the vortices here are round due to scattering by the S impurities. As shown in the tunneling conductance curves, at different distances from the core center (Fig. 5), there is a zero bias peak. The zero bias peak is smeared due to scattering by the S substitution with respect to the pure compound. Previous measurements in Ref. [35] show the decrease of the zero bias peak in the vortex core when substituting Nb by Ta. In the 2H-NbSe$_{1.8}$S$_{0.8}$, the zero bias peak is strongly depressed.

We have also measured spatial distributions $N(r,\epsilon)$ at finite bias energies ϵ. In Fig. 6 we show the angular averaged $N(r,\epsilon)$ for all three compounds. Note that the shape of the conductance vs bias voltage remains roughly the same in increasing fields in β-Bi$_2$Pd, whereas for the other two compounds the conductance tends to increase away from the core with increasing H. This tendency is seen by comparing the curves obtained from the zero bias data in Figs. 2 and 3 of the main text.
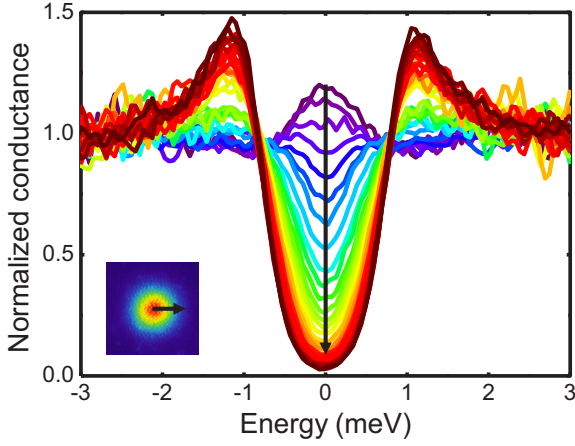
FIG. 5. Tunneling conductance vs position at $H = 0.02$ T in 2H-NbSe$_{1.8}$S$_{0.2}$ along the line given by the black arrow in the inset, which is a zero-bias conductance map of a vortex.

APPENDIX B: VORTEX CORE STATES

The tunneling conductance within the vortex core shows zero-bias peaks in 2H-NbSe$_{1.8}$S$_{0.2}$ and in 2H-NbS$_2$ due to Caroli-deGennes-Matricon core bound states. We do not take these peaks into account in our model. The core states provide a zero-bias conductance slightly above one (see Fig. 5 for 2H-NbSe$_{1.8}$S$_{0.2}$ and Ref. [15] for 2H-NbS$_2$). The shape of the vortex core is not significantly affected by these peaks. Note that in the paper we calculate σ according to Eq. (1). Hence, the magnetic field dependence of $\sigma_0(0)$ and of $\sigma_0(r^*)$ do not influence σ.

On the other hand, in the previous work [15] we have demonstrated that the absence of the core starlike anisotropy in 2H-NbS$_2$ is due to the absence of charge density waves (CDW) in this compound. Thus, CDW causes the in-plane anisotropy of the vortex core in 2H-NbSe$_2$ [15]. Here, we observe the CDW also in 2H-NbSe$_{1.8}$S$_{0.2}$ (Fig. 7). The loss of in-plane anisotropy is shown here for the first time. Previous measurements have studied Ta$_{1-x}$Nb$_x$Se$_2$. Authors of that paper find that the height of the zero bias quasiparticle peak decreases with substitution, although the effect of scattering on the in-plane core anisotropy was not addressed.

APPENDIX C: SAMPLE GROWTH OF 2H-NbSe$_{1.8}$S$_{0.2}$

The synthesis of 2H-NbSe$_{1.8}$S$_{0.2}$ was performed in a typical solid state reaction. The elements were mixed in
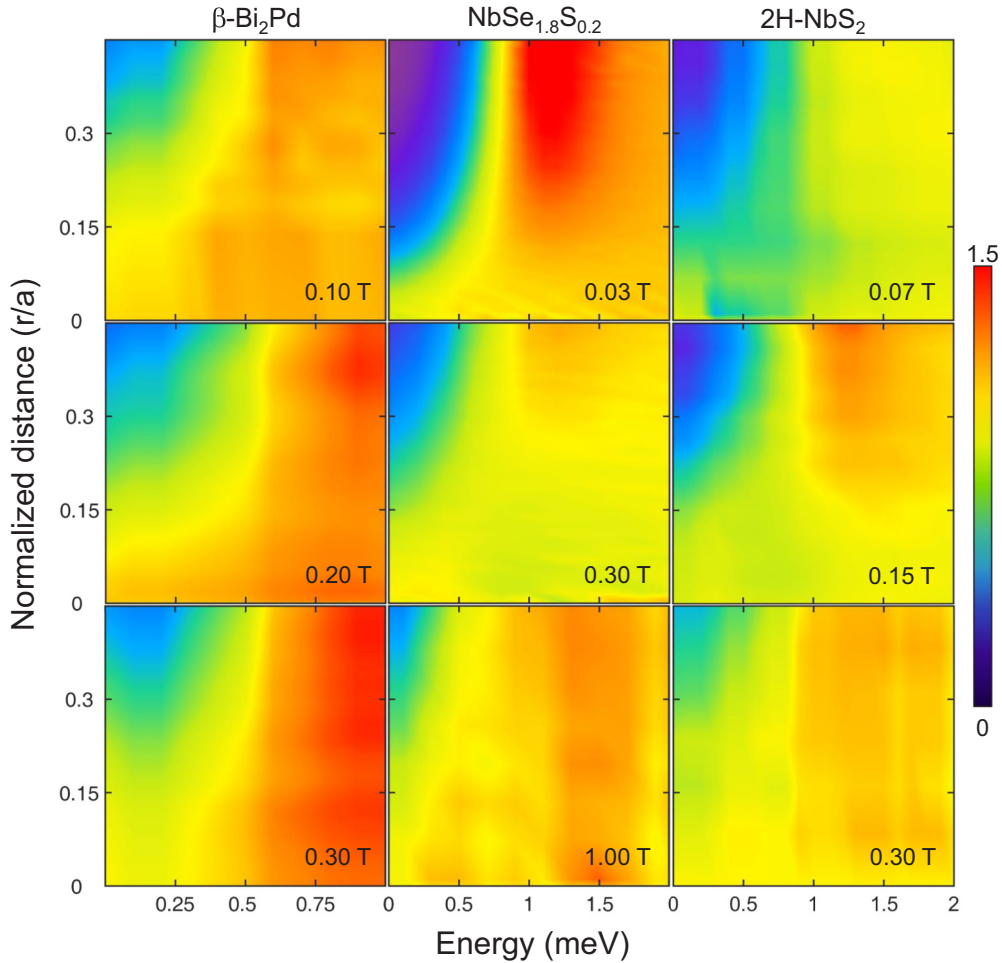

FIG. 6. The angular averaged conductance normalized at its value at high bias voltages plotted as a function of distance r/a (with a being the half intervortex distance) and the bias voltage at magnetic fields marked in the figure.
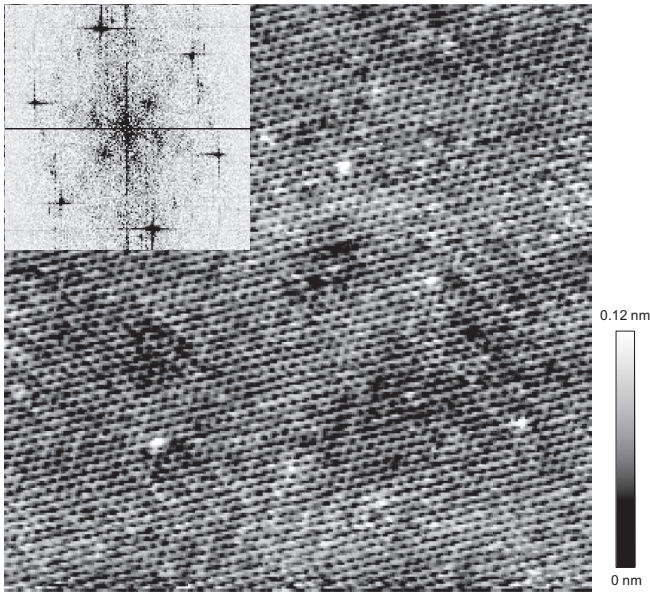
FIG. 7. Atomic resolution topography of 2H-NbSe$_{1.8}$S$_{0.2}$ showing the CDW in area with a lateral size of 20 nm. The Fourier transform is shown in the inset. The CDW wave vectors are indistinguishable, within experimental error, from the pure compound. The modulation is threefold, with $q = 0.29$ 1/Å for the atomic lattice and 0.085 1/Å for the CDW, within an error of 20%. The CDW is located at a distance of 34% of the atomic lattice, i.e., 1/3 within accuracy of the relative values, which we estimate to be around 5% from the width of the Fourier transform peaks. Note also that there are sizable variations in topographic contrast that are certainly due to scattering by S defects.
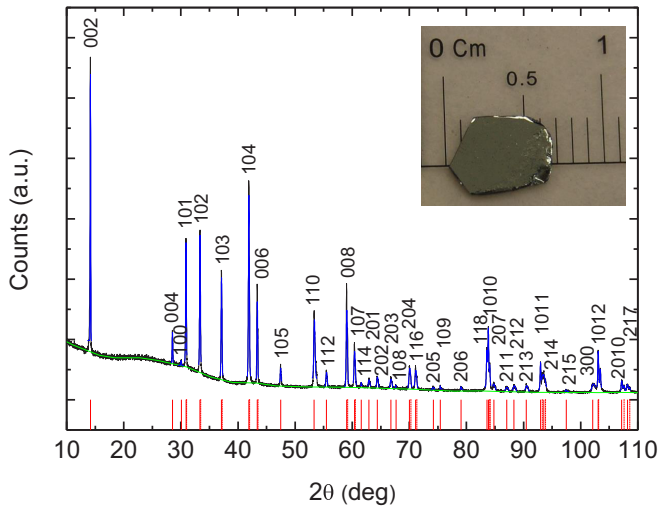

FIG. 8. XRPD experimental pattern of 2H-NbSe$_{1.8}$S$_{0.2}$ single crystal (black) and corresponding fit (peaks in blue and background in green). The fit gives: $a = b = 3.4323(3)$ Å and $c = 12.513(1)$ Å, a hexagonal crystal system with $P63/mmc$ space group, $X^2 = 2.22 \times 10^{-5}$, and a Snyder's figure of merit of 44.3158. Inset: view of the grown single crystal.
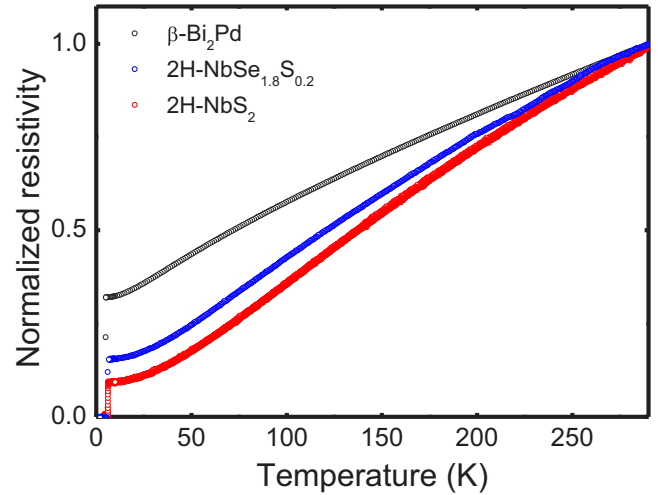

FIG. 9. Temperature dependence of the resistivity for β-Bi$_2$Pd, 2H-NbSe$_{1.8}$S$_{0.2}$, and 2H-NbS$_2$ normalized to the ambient temperature value.

a stoichiometric ratio, sealed inside the evacuated quartz ampoule and heated from room temperature up to 900 °C at 1.5 °C/min. The sample was kept at constant temperature during 14 days and then was slowly cooled down (0.07 °C/min). To obtain large single crystals, we mixed four mmol with I$_2$ as a transport agent ([I$_2$] $\approx$ 5 mg/cm^3) in evacuated quartz tube, which was placed inside a three-zone furnace. We placed the material in the leftmost zone and heated the other two zones for three hours up to 700 °C and kept them at this temperature for one day. After that, the leftmost zone was heated to 750 °C within three hours and we established temperature gradients as 750 °C/700 °C/725 °C. These temperatures were kept for 22 days after which the oven was switched off for cooling.

The crystals so formed were analyzed by inductively coupled plasma spectrometry and by powder x-ray diffraction (Fig. 8). The elements content was Nb:36.9 ±1.0%, Se:58.8 ±1.5%, and S:2.4 ± 0.2% in good agreement with the expected values for 2H-NbSe$_{1.8}$S$_{0.2}$. Refinement of the x-ray pattern revealed a hexagonal lattice with a $P63/mmc$ space group and a unit cell of $a = b = 3.4323(3)$Å, $c = 12.513(1)$Å, $\alpha = \beta = 90°$, and $\gamma = 120°$. These results are only slightly different from those for pure 2H-NbSe$_2$ [$a = b = 3.4425(5)$Å, $c = 12.547(3)$Å, $\alpha = \beta = 90°$, and $\gamma = 120°$] [36].

APPENDIX D: RESISTIVITY OF β-Bi$_2$Pd, 2H-NbSe$_{1.8}$S$_{0.2}$, AND 2H-NbS$_2$

In Fig. 9 we provide the temperature dependence of the resistivities normalized to the ambient temperature value for the three compounds studied in this paper.

[1] V. G. Kogan and N. V. Zhelezina, Field dependence of the vortex core size, Phys. Rev. B **71**, 134505 (2005).

[2] J. E. Sonier, Investigations of the core structure of magnetic vortices in type-II superconductors using muon spin rotation, J. Phys.: Condens. Matter **16**, S4499 (2004).

[3] V. G. Kogan, R. Prozorov, S. L. Bud'ko, P. C. Canfield, J. R. Thompson, J. Karpinski, N. D. Zhigadlo, and P. Miranović, Effect of field-dependent core size on reversible magnetization of high-κ superconductors, Phys. Rev. B **74**, 184521 (2006).

[4] U. Klein, Density of states in the vortex state of type-II superconductors, Phys. Rev. B **40**, 6601 (1989).

[5] N. Nakai, P. Miranovic, M. Ichioka, H. F. Hess, K. Uchiyama, H. Nishimori, S. Kaneko, N. Nishida, and K. Machida, Ubiquitous V-Shape Density of States in a Mixed State of Clean Limit Type II Superconductors, Phys. Rev. Lett. **97**, 147001 (2006).

[6] F. Gygi and M. Schlüter, Self-consistent electronic structure of a vortex line in a type-II superconductor, Phys. Rev. B **43**, 7609 (1991).

[7] P. J. Hirschfeld, M. M. Korshunov, and I. I. Mazin, Gap symmetry and structure of Fe-based superconductors, Rep. Prog. Phys. **74**, 124508 (2013).

[8] O. Fischer, M. Kugler, and I. Maggio-Aprile, Scanning tunneling spectroscopy of high-temperature superconductors, Rev. Mod. Phys. **79**, 353 (2007).

[9] H. Suderow, I. Guillamón, J. G. Rodrigo, and S. Vieira, Imaging superconducting vortex core and lattices with a scanning tunneling microscope, Supercond. Sci. Technol. **27**, 063001 (2014).

[10] H. F. Hess, R. B. Robinson, R. C. Dynes, J. M. Valles, and J. V. Waszczak, Scanning-Tunneling-Microscope Observation of the Abrikosov Flux Lattice and the Density of States near and inside a Fluxoid, Phys. Rev. Lett. **62**, 214 (1989).

[11] H. F. Hess, R. B. Robinson, and J. V. Waszczak, Vortex-Core Structure Observed with a Scanning Tunneling Microscope, Phys. Rev. Lett. **64**, 2711 (1990).

[12] P. G. de Gennes, Behavior of dirty superconductors in high magnetic fields, Phys. Kond. Materie **3**, 79 (1964).

[13] K. Maki, in *Superconductivity*, edited by R. D. Parks (Marcell Dekker, New York, 1969), Vol. 2, p. 1086.

[14] E. Herrera, I. Guillamón, J. A. Galvis, A. Correa, A. Fente, R. F. Luccas, F. J. Mompéan, M. García-Hernández, S. Vieira, J. P. Brison, and H. Suderow, Magnetic field dependence of the density of states in the multiband superconductor β-Bi$_2$Pd, Phys. Rev. B **92**, 054507 (2015).

[15] I. Guillamón, H. Suderow, S. Vieira, L. Cario, P. Diener, and P. Rodiere, Superconducting Density of States and Vortex Cores of 2H-NbS$_2$, Phys. Rev. Lett. **101**, 166407 (2008).

[16] I. Guillamón, H. Suderow, F. Guinea, and S. Vieira, Intrinsic atomic-scale modulations of the superconducting gap of 2H-NbS$_2$, Phys. Rev. B **77**, 134505 (2008).

[17] D. Saint-James, G. Sarma, and E. J. Thomas, *Type-II Superconductivity* (Pergamon, Oxford, 1969), Eq. (6.83).

[18] C. Caroli, P. G. deGennes, and J. Matricon, Bound Fermion states on a vortex line in a type II superconductor, Phys. Lett. **9**, 307 (1964).

[19] G. Eilenberger, Transformation of Gorkov's Equation for Type II Superconductors into Transport-Like Equations, Z. Phys. **214**, 195 (1968).

[20] In fact, the same relation holds for the clean case subject to certain restrictions which affect the coefficient by $|\Delta|^2$, see P. deGennes and S. Mauro, Sol. St. Comm. **3**, 381 (1965).

[21] A. Schmid, A time dependent Ginzburg-Landau equations and its application to the problem of resistivity in the mixed state, Phys. Kond. Materie **5**, 302 (1966).

[22] J. R. Clem, Simple model for the vortex core in a type II superconductor, J. Low Temp. Phys. **18**, 427 (1975).

[23] Z. Hao, J. R. Clem, M. W. McElfresh, L. Civale, A. P. Malozemoff and F. Holtzberg, Model for the reversible magnetization of high-K type-II superconductors: Application to high-T_c superconductors, Phys. Rev. B **43**, 2844 (1991).

[24] M. D. Johannes, I. I. Mazin, and C. A. Howells, Fermi-surface nesting and the origin of the charge-density wave in 2H-NbSe$_2$, Phys. Rev. B **73**, 205102 (2006).

[25] V. G. Tissen, M. R. Osorio, J. P. Brison, N. M. Nemes, M. García-Hernández, L. Cario, P. Rodière, S. Vieira, and H. Suderow, Pressure dependence of superconducting critical temperature and upper critical field of $2H$-NbS$_2$, Phys. Rev. B **87**, 134502 (2013).

[26] B. T. Geilikman, R. O. Zaitsev, and V. Z. Kresin, Properties of Superconductors Having Overlapping Bands, Solid State Phys. **9**, 642 (1967) [Fizika Tverdogo Tela **9**, 821 (1967)]; V. Z. Kresin, Transport properties and determination of the basis parameters of superconductors with overlapping bands, J. Low Temp. Phys. **11**, 519 (1973).

[27] J. Geyer, R. M. Fernandes, V. G. Kogan, and J. Schmalian, Interface energy of two-band superconductors, Phys. Rev. B **82**, 104521 (2010).

[28] V. G. Kogan and J. Schmalian, Ginzburg-Landau theory of two-band superconductors: Absence of type-1.5 superconductivity, Phys. Rev. B **83**, 054515 (2011).

[29] L. Komendova, Y. Chen, A. A. Shanenko, M. V. Milošević, and F. M. Peeters, Two-Band Superconductors: Hidden Criticality Deep in the Superconducting State, Phys. Rev. Lett. **108**, 207002 (2012).

[30] H. Suderow, I. Guillamón, and S. Vieira, Compact very low temperature scanning tunneling microscope with mechanically driven horizontal linear positioning stage, Rev. Sci. Instrum. **82**, 033711 (2011).

[31] J. A. Galvis *et al.*, Three axis vector magnet set-up for cryogenic scanning probe microscopy, Rev. Sci. Instrum. **86**, 013706 (2015).

[32] I. Guillamón, H. Suderow, S. Vieira, and P. Rodiere, Scanning tunneling spectroscopy with superconducting tips of Al, Physica C **468**, 537 (2008).

[33] J. G. Rodrigo, H. Suderow, and S. Vieira, On the use of STM superconducting tips at very low temperatures, Eur. Phys. J. **40**, 483 (2004).

[34] J. G. Rodrigo, H. Suderow, S. Vieira, E. Bascones, and F. Guinea, Superconducting nanostructures fabricated with the scanning tunneling microscope, J. Phys. Condens. Matter **16**, R1151 (2004).

[35] Ch. Renner, A. D. Kent, Ph. Niedermann, O. Fischer, and F. Levy, Scanning tunneling spectroscopy of a vortex core from the clean to the dirty limit, Phys. Rev. Lett. **67**, 1650 (1991).

[36] A. Meerschaut and C. Deudon, Crystal structure studies of the 3R-Nb$_{1.09}$S$_2$ and the 2H-NbSe$_2$ compounds: correlation between nonstoichiometry and stacking type (= polytypism), Mater. Res. Bull. **36**, 1721 (2001).